Magnetotransport in epitaxial thin films of the magnetic perovskite $Pr_{0.5}Sr_{0.5}MnO_3$

P. H. Wagner, V. Metlushko,* and L. Trappeniers
Laboratorium voor Vaste-Stoffysica en Magnetisme, Katholieke Universiteit Leuven, Celestijnenlaan 200 D, 3001 Leuven, Belgium

A. Vantomme
Instituut voor Kern-en Stralingsfysica, Katholieke Universiteit Leuven, Celestijnenlaan 200 D, 3001 Leuven, Belgium

J. Vanacken
Laboratorium voor Vaste-Stoffysica en Magnetisme, Katholieke Universiteit Leuven, Celestijnenlaan 200 D, 3001 Leuven, Belgium and Tsukuba Magnet Laboratories, National Research Institute for Metals, Sengen 1-2-1, Tsukuba Science City, Ibaraki 305, Japan

G. Kido
Tsukuba Magnet Laboratories, National Research Institute for Metals, Sengen 1-2-1, Tsukuba Science City, Ibaraki 305, Japan

V. V. Moshchalkov and Y. Bruynseraede
Laboratorium voor Vaste-Stoffysica en Magnetisme, Katholieke Universiteit Leuven, Celestijnenlaan 200 D, 3001 Leuven, Belgium
(Received 28 March 1996; revised manuscript received 4 October 1996)

Thin, $\vec{c}$-axis oriented films of the magnetic perovskite $Pr_{0.5}Sr_{0.5}MnO_3$ were prepared by dc-magnetron sputtering, structurally characterized by x-ray diffraction and their physical properties investigated by magnetization and electrical transport measurements. Ferromagnetic ordering appears in zero field at 263 K, followed by a second transition into an antiferromagnetic state at 160 K. The zero-field resistivity has a semiconducting behavior above the Curie and below the Néel temperature and is analyzed in the framework of Mott's variable range hopping concept. Quasimetallic behavior is observed within the ferromagnetic state, whose temperature range can be extended by applying an external magnetic field. The negative magnetoresistance effect increases systematically with decreasing temperature and reaches a value of 700% at 1.5 K in a field of 12 T. In the ferro- and antiferromagnetic phases, the field induced resistivity decrease scales with the Brillouin function, suggesting the existence of magnetically polarized regions with a total magnetic moment which is reduced upon entering the antiferromagnetic state.
[S0163-1829(97)01905-X]

I. INTRODUCTION

Manganese perovskites $RMnO_3$ with trivalent rare-earth ions R^{3+} are antiferromagnetic (AFM) insulators. Doping with divalent ions on the site of the trivalent R^{3+} results in a metallic conductivity and a ferromagnetic (FM) ordering.[1] The recent discovery of giant negative magnetoresistance (GMR) in $La_{0.67}Ba_{0.33}MnO_3$ and $Nd_{0.5}Pb_{0.5}MnO_3$ (Refs. 2 and 3) has increased considerably the interest in the manganese perovskites $RMnO_3$, in particular in compounds with R=La, Nd. Above the Curie temperature T_C the doped La and Nd manganites are paramagnetic (PM) semiconductors and undergo at T_C a transition to a ferromagnetic metallic state. This state persists down to the lowest temperatures, while the maximum of the GMR effect shows up around T_C.[4] The conductivity is supposed to emerge from hopping of magnetic polarons above T_C,[2,3] and from the double-exchange mechanism below T_C.[5–7] The analytical dependence of the GMR effect versus external field is not yet fully understood, but correlations between magnetization and resistivity in La manganites suggest an important role of the polaron hopping also below T_C.[8]

Another manganite compound, $Pr_{0.5}Sr_{0.5}MnO_3$, behaves somewhat differently: neutron-diffraction studies of semiconducting, polycrystalline $Pr_{0.5}Sr_{0.5}MnO_3$ revealed again ferromagnetism below 200 K, followed however by a coexistence of the FM and AFM phases between 80 K and 160 K, and a purely AFM phase below 80 K.[9] Magnetization and transport measurements on a high-quality single crystal confirmed the presence of the two transitions with a $T_C = 270$ K and a Néel temperature $T_N = 140$ K.[10] The transition from the FM to the AFM state in the single crystal is probably first order, while the conductivity is metallic in the FM and semiconducting in the AFM phase. Based on the jumplike resistivity increase at the transition from the FM to the AFM state, and a particular doping state with exactly 0.5 charge carriers per Mn ion, it was speculated that the weakly localized carriers in the $Pr_{0.5}Sr_{0.5}MnO_3$ single crystal undergo a charge ordering transition into an insulating, antiferromagnetic Wigner crystal.[10] The origin of this low-temperature AFM behavior of the Pr manganite is related to the weakening of the ferromagnetic Mn^{3+}-Mn^{4+} superexchange coupling by the contraction of the chemical unit cell. Moreover Pr exhibits intrinsic mixed-valency properties, with a magnetic moment of $3.5\mu_B$ for Pr^{3+}, while La^{3+} is nonmagnetic.[11]

The purpose of this work is to investigate the transport properties of the $Pr_{0.5}Sr_{0.5}MnO_3$ perovskite films. We shall

also consider closely the assumed occurence of Wigner crystallization by carrying out a quantitative analysis of the observed resistance behavior together with an identification of the underlying conductivity mechanism. According to our knowledge, a theoretically well-founded resistivity scaling which would enable one to identify the charge ordered phase, has not yet been developed. Besides these main objectives, also the transition from the semiconducting-paramagnetic to the FM-metallic state, common to La as well as Pr manganites, requires additional analysis. We shall investigate further the idea that polaronlike carriers may contribute to the conductivity also below T_C, and that double exchange, restricted to nearest-neighbor Mn sites, needs not to be an exclusive way for charge transport. This means that charge exchange between Mn sites of arbitrary distance might be possible, provided only that Hund's rules are obeyed. These ideas for the conductivity mechanism will be pursued by analyzing resistance versus external magnetic fields employing a polaronic hopping model. For the experiments discussed within this work we used an epitaxial film, which offers the advantage of coming close to the quality of single crystals, thus close to the intrinsic properties of the material. Furthermore, thin films represent the most feasible sample form for potential device applications and the preparation of multilayers.

II. SAMPLE PREPARATION

Starting from a polycrystalline, disk-shaped target with the nominal composition $Pr_{0.50}Sr_{0.50}Mn_{1.00}O_{\approx 3}$, thin films were deposited onto $SrTiO_3$ (1 0 0) substrates by on-axis dc-magnetron sputtering. The target was prepared by thoroughly mixing stoichiometric amounts of Pr_6O_{11}, $SrCO_3$, and $MnCO_3$, calcinating (12 h at 900 °C) and firing in air (24 h at 1250 °C) with intermediate grinding. After pulverizing the reacted material, the powder was moistened with isopropanol and pressed into a 2 mm thick disk (38 mm diameter) with 40 MPa uniaxial pressure. The target was dried and sintered in air for 24 h at 1250 °C and an additional 6 h at 1350 °C. During the sputtering of the films (120 min for a 3000 Å thick layer) the discharge current was 100 mA (-290 V) in a 1.5 hPa flowing oxygen atmosphere, and with a target-substrate distance of 20 mm. The $SrTiO_3$ substrates ($10\times10\times1$ mm^3) were glued with silver paint to an Al_2O_3 block, which was resistively heated up to $\approx$ 900 °C in order to achieve epitaxial film growth. The actual temperature at the substrate surface is estimated to be 200 °C lower. Higher deposition temperatures resulted in polycrystalline films, a structure which was also observed for films deposited on (1 0 0) oriented MgO irrespective of the deposition temperature. Although the phase formation is complete after deposition, the films were kept an additional 30 min in 10 hPa O_2 at 900 °C, and 30 min in 500 hPa O_2 at 600 °C, in order to achieve a homogeneous oxidization.

The x-ray diffraction spectra obtained with the Bragg-Brentano geometry show that the films have no extra phases and are $\vec{c}$-axis oriented with FWHM values (full width at half maximum) for the Θ scan of the (0 0 2) reflection between 0.19° and 0.39° (Fig. 1). For the sample discussed in the following sections the FWHM was 0.37°, indicating an excellent structural order, comparable to the FWHM $\approx$0.15°

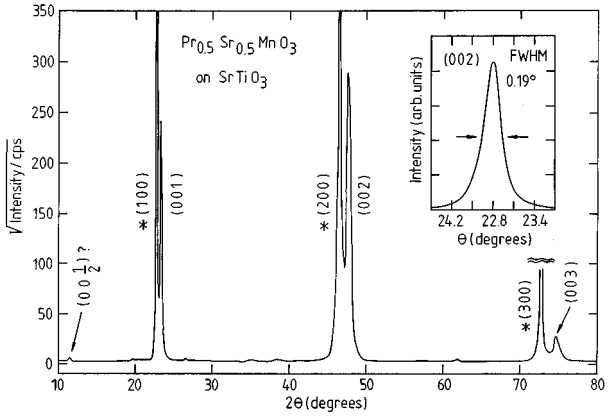

FIG. 1. X-ray diffraction spectrum in Bragg-Brentano geometry of an epitaxial $Pr_{0.5}Sr_{0.5}MnO_3$ film on a $SrTiO_3$ (1 0 0) substrate. The small reflection at 11.44° belongs to the superstructure along the c axes, while the inset shows the Θ scan of (0 0 2). Reflexes of the substrate are indicated by $\star$.

for the (2 0 0) reflection of the single-crystalline $SrTiO_3$ substrates. The averaged lattice constant, obtained from the peak position at the (0 0 3) reflections of three different films, is 3.818 $\pm$ 0.002 Å, in good agreement with the half c-axis length determined with neutron diffraction, i.e., 7.644 Å.[9] The difference by a factor of 2 arises from the special sensitivity of neutron diffraction to a superstructure, caused by deviations from the ideal cubic perovskite lattice. The small reflection visible at 11.44°, see Fig. 1, is probably due to this superstructure with a calculated lattice constant of 7.73 Å. The half diagonal of the ab plane of the superstructure is 3.842 Å,[9] in good agreement with the lattice constant of the $SrTiO_3$ substrate (3.905 Å). Therefore a strong in-plane texture can be expected, and $\vec{a}$- or $\vec{b}$-axis oriented film growth has not been observed.

The interface between film and substrate surface has not been investigated yet, but from the slight lattice mismatch we suppose that the film properties might be influenced to some extent by strain. Chemical interdiffusion probably does not play an important role, because Sr and O are also ingredients of the $Pr_{0.5}Sr_{0.5}MnO_3$ and Ti might substitute Mn, due to similar ionic radii. In $Bi_2Sr_2CaCu_2O_{8+\delta}$ films deposited onto $SrTiO_3$ by almost the same sputtering technique as described above, Ti was found to interdiffuse not more than 500 Å into the growing film.[12] Considering the total film thickness of 3000 Å the interface will have only a small influence on the measured properties of the whole film volume. Scanning electron microscopy of the $Pr_{0.5}Sr_{0.5}MnO_3$ films showed no trace of particles on the mirrorlike surfaces, while the average roughness of a 1 μm^2 surface obtained with atomic force microscopy is 40 Å for a 3000 Å thick film. Composition analysis by means of Rutherford backscattering revealed the ratio $Pr_{0.5}Sr_{0.5}Mn_{1.25}O_{\approx 3}$ with an uncertainty of about 10% for the cations. The origin of the Mn surplus is not yet clear and might be caused by the influence of the magnetic field onto the manganese atoms in the magnetron-assisted discharge plasma, forming amorphous, Mn-rich second phases on the substrate.

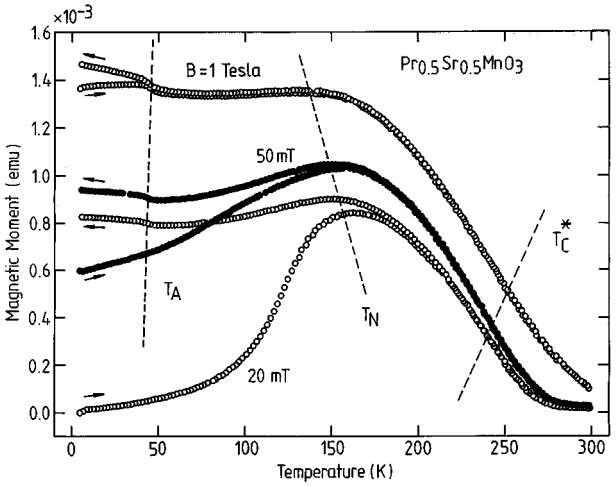

FIG. 2. In-plane magnetic moment of a $Pr_{0.5}Sr_{0.5}MnO_3$ film vs temperature for magnetizing fields of 20 mT, 50 mT, and 1 T in warming and cooling runs as indicated by arrows. The lines suggest the positions of (i) the Curie temperature $T_C^{\star}$ of ferromagnetism, (ii) the onset temperature T_N of antiferromagnetic correlations, and (iii) the low-temperature anomaly T_A as discussed in the text.

III. MAGNETIC PROPERTIES OF THE $Pr_{0.5}Sr_{0.5}MnO_3$ FILMS

The in-plane sample magnetization M was measured with a Quantum Design SQUID in fields between 20 mT and 5 T. Prior to applying a field, the sample was cooled from 300 K to 5 K in zero field in order to ensure equivalent preconditions for each measurement. The measurements were then performed by warming up to 300 K with subsequent cooling to 5 K. Figure 2 shows representative $M(T)$ curves for 20 mT, 50 mT, and 1 T, all data points being corrected for the small diamagnetic response of the $SrTiO_3$ substrate. Higher magnetic fields did not substantially alter the appearance of the data for 1 T. The mean-field ferromagnetic Curie temperature T_C was determined by linearly extrapolating the $M(T)^{-1}$ data to zero. For 20 mT, close to the zero-field limit, we obtained $T_C = 263$ K, comparable to 270 K as reported for the $Pr_{0.5}Sr_{0.5}MnO_3$ single crystal by Tomioka *et al.*[10] By applying external fields, T_C is shifted slightly to higher temperatures. Although in the presence of fields higher than 20 mT no clear Curie-Weiss behavior was found in the data, allowing to determine T_C by a linear extrapolation, this shift is also reflected by the shift of $T_C^{\star}$, defined as the high-temperature inflection point of $M(T)$, as shown in Fig. 2. The transition to the AF state occurs around $T_N = 160$ K (B_{ext}=20 mT) as clearly indicated by the reduction of M with decreasing T.[13] This implies that the Mn^{3+} and Mn^{4+} ions form independently two AF sublattices, if we assume different moments for Mn^{4+} ($4.0\mu_B$) and Mn^{3+} ($5.0\mu_B$), according to Ref. 11. Knížek *et al.*[9] also reported two AF sublattices, however with almost identical moments of $2.24\mu_B$ (Mn^{4+}) and $2.20\mu_B$ (Mn^{3+}). With increasing external field the local magnetization maximum at T_N is less pronounced and shifts to slightly lower temperatures. The field dependence of T_N and T_C will be further discussed in connection with the resistivity data in Sec. V A. The onset of the AF behavior (Fig. 2) is at all fields accompanied by a splitting of the cooling and the warming magnetization data, a phenomenon also showing up in the resistivity measurements. A possible explanation may be that in the cooling mode the spin system is thermally stronger activated and thus more flexible to be aligned in the direction of the external field. This results in higher magnetization values, combined with a lowered resistivity, as the spin system gains an enhanced ferromagnetic component.

We note that the magnetic moment of the sample measured in 1 T at 5 K (1.5×10^{-3} emu, i.e., 100 emu/cm^3 with an uncertainty of 10%), corresponds to $0.62\mu_B$ per Mn ion. This is considerably below the above-mentioned values, calculated on the basis of the Mn ion spins, while films of the La manganites exhibit moments close to 50% of the theoretical value.[2] Higher external fields do not change substantially the $M(T)$ data, because the coercitive fields deduced from magnetization loops are in the range of only 100 mT and saturation is apparently achieved already for external fields in the range of 1 T. This is in contradiction with the transport measurements, see Sec. V A below, where fields of 12 T are not sufficient to achieve saturation of the GMR effect. A probable explanation for this dicrepancy is the existence of magnetic domains: Magnetization measurements are sensitive to the magnetic moment of the whole sample, integrated over different domains, while resistance measurements probe the scattering of carriers within and between all individual domains. An imperfect ordering of the spin lattices, including magnetically ordered clusters embedded in a paramagnetic matrix, may also be responsible for the observed difference.

At $T_A \approx 45$ K (see Fig. 2) a small jump in the magnetization is observed, especially in the cooling runs. Several mechanisms may cause this jump: (i) a transition from two independent AFM sublattices for Mn^{3+} and Mn^{4+} to two FM lattices, resulting in ferrimagnetism; (ii) an ordering of the Pr^{3+} moments; and (iii) the presence of magnetically ordering second phases. The first possibility can be excluded since the calculated moment per Mn ion exceeds the half difference between Mn^{3+} and Mn^{4+} spin moments. Concerning the second possibility, it is well known that the Pr moments in $PrBa_2Cu_3O_7$ undergo antiferromagnetic ordering with a Néel temperature of 17 K,[14] comparable to the 40 K observed for the $Pr_{0.5}Sr_{0.5}MnO_3$ films. Also in the $Nd_{0.5}Pb_{0.5}MnO_3$ system a susceptibility anomaly showed up at 30 K, which was associated with ordering in the Nd^{3+} lattice ($3.5\mu_B$) and enhanced carrier localization.[3] The most likely explanation seems to be the presence of (amorphous) traces of the Mn-rich $PrMn_2O_5$ phase with $T_N = 46$ K.[15] X-ray diffraction (XRD) reflections corresponding to the lattice constants of this compound (see Ref. 16) were not detected for the sample under investigation, therefore we conclude the volume fraction to be below 10%.

IV. ZERO-FIELD RESISTIVITY OF THE $Pr_{0.5}Sr_{0.5}MnO_3$ FILMS

A. Experimental results

In order to obtain a meaningful comparison between electrical and magnetic properties, the transport measurements were performed on a strip cut from the same film which was also used for the magnetization measurements. Due to difficulties in patterning $Pr_{0.5}Sr_{0.5}MnO_3$ by chemical etching, we

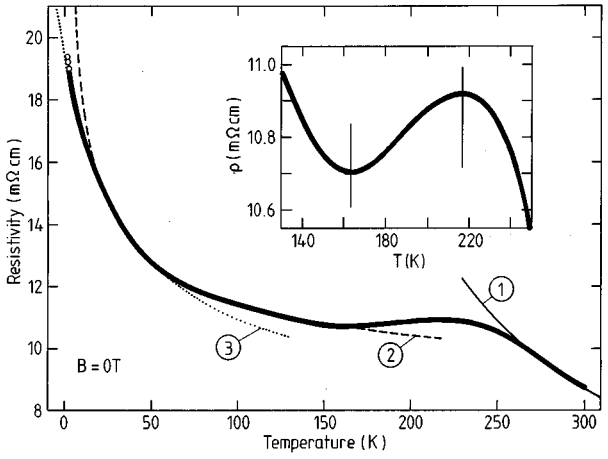

FIG. 3. Zero-field resistivity as a function of temperature of a $Pr_{0.5}Sr_{0.5}MnO_3$ film. Fitting of the experimental data was done according to (1) thermally activated nearest-neighbor hopping in the paramagnetic phase, (2) variable range hopping in the antiferromagnetic phase below 160 K, and (3) the empirical low temperature scaling $\rho \propto \exp[\Theta_1/(T+\Theta_2)]$. The inset shows a detail of the apparently metallic (ferromagnetic) regime, with perpendicular lines indicating the transition temperatures $T_N \approx$ 160 K and $T_C \approx$ 220 K.

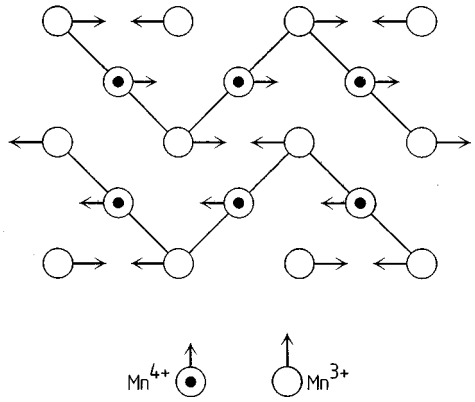

FIG. 4. Antiferromagnetic, CE-type spin structure of $Pr_{0.5}Sr_{0.5}MnO_3$ at low temperatures according to Refs. 9 and 24. The spins are projected into the plane to illustrate the existence of conducting paths, shown as solid lines.

measured the unpatterned strip (10 mm long, 2.8 mm wide) after evaporating four gold contacts (2.8 mm × 1 mm, 6 mm distance between the voltage probes) in one line across the sample and annealing them in air for 15 min at 700 °C. These contacts were stable against thermal cycling and had a contact resistance below 1 Ω. For the measurements discussed in the following subsections we employed an ac bridge (28 Hz) at an effective excitation current of 0.3μA. The current direction was within the *ab* plane of the film, parallel to the orientation of the external magnetic field, thus in the Lorentz-force free configuration. Preliminary measurements under different angles between the $\vec{c}$ axis and the field direction suggest a magnetically isotropic behavior.[17]

Figure 3 shows the temperature dependence of the zero-field resistivity, with a magnification of the metalliclike region between 160 K and 220 K in the inset. The observed temperature dependence is in agreement with the single crystal data reported by Tomioka *et al.*,[10] including comparable resistivity values, except for the smooth quasimetallic to semiconducting transition at 160 K. Above the metalliclike region ($T>250$ K) the resistivity scales with thermally activated nearest-neighbor hopping [$\rho \propto \exp(U/k_BT)$, $U \approx 30$ meV], which can be attributed to magnetic polarons, as assumed for the doped Nd and La manganites.[2,3] Below the metallic region (50 K $<T<$ 160 K) a semiconducting behavior is observed in accordance with Mott's law for variable range hopping (VRH), i.e., $\ln\rho \propto (\Theta/T)^{1/4}$.[18] In a more detailed investigation of this temperature region in Sec. IV B, we will also take into account the slight temperature dependence of the corresponding proportionality factor. Below 50 K the resistivity starts to deviate from Mott's law and scales with $\ln\rho \propto \Theta_1/(T+\Theta_2)$ ($\Theta_1 = 54.9$ K, $\Theta_2 = 60.0$ K). This functional dependence for $T \leqslant 50$ K resembles the susceptibility of an antiferromagnet above T_N and remains valid also in the presence of external magnetic fields, with slightly other values for Θ_1 and Θ_2. Although there is no theoretical model for this peculiar $\rho(T)$ behavior, the correspondence of the empirical relation with the data is excellent and superior to fit functions based on Mott- or Shklovskii-Efros hopping. The existence of two different scaling regimes below 160 K indicates again a change in magnetic ordering around 50 K, in accordance with the magnetization data.

B. Discussion of the zero-field resistivity data

1. Semiconducting behavior through Wigner crystallization

The double-exchange mechanism in the doped rare-earth manganites provides below T_C delocalized carriers,[5–7] scattered by phonons and spin waves, resulting in metallic behavior as known already for the La and Nd compounds.[2,3] Resistivity seems to scale with the temperature dependent strength of the double-exchange interaction, which is correlated with the total magnetization of the system. The new feature of a resistivity increase below 160 K observed for the $Pr_{0.5}Sr_{0.5}MnO_3$ compound is accompanied by an antiferromagnetic and also geometric ordering of Mn ions, with Mn^{3+} and Mn^{4+} occupying two cubic sublattices. The semiconducting behavior originates therefore from either the Coulomb repulsion between charge carriers, or from the antiferromagnetic spin arrangement.

The antiferromagnetism of ''collinear CE-type,''[9] see Fig. 4, destroys partially the ferromagnetic, parallel alignment of neighboring moments in the sense that each Mn^{3+} ion will sit within the *ab* plane in the center of a square with adjacent corners formed by two Mn^{4+} ions with spin parallel and two with spin antiparallel to the Mn^{3+} moment. Due to the Hund coupling carrier exchange is hindered between Mn^{3+} and the antiparallel Mn^{4+} ions, while it is still allowed for the parallel Mn^{4+} sites. As a result, the carriers will remain delocalized on zigzaglike paths along a definite axis of the Wigner crystal and strongly localized in the perpendicular in-plane direction. In the thin films, the Mn^{3+}/Mn^{4+} lattice is probably disturbed and therefore one expects a mixture of both orientations. Antiferromagnetism alone is thus probably not sufficient to bring about the transition from a metallic to an insulating phase, but can account for a resistivity increase.

In the original idea of Wigner crystallization, the resistivity increase arises from the mutual repulsion between carri-

ers, freezing in regular sublattices. Since the resistivity remains finite down to the lowest temperature, for the thin film as well as for the single crystal,[10] one can suppose the remanent conductivity to be determined by a certain density of defects in the charge crystal. This defect density should follow a thermally activated behavior with an activation energy in the order of the Coulomb potential between neighboring carriers.[18] In a rough calculation, this energy is in the order of 2×10^4 K, and by taking into account shielding effects through a dielectric constant in the order of 10^2, it cannot be supposed to be smaller than 200 K. However, our data deviate in the low-temperature region considerably from the thermally activated Arrhenius scaling, and Wigner crystallization in a strict sense is thus improbable.

2. Semiconductivity based on variable range hopping

Regarding the semiconducting behavior of resistivity above 220 K and below 160 K, it is tempting to analyze the whole zero-field temperature dependence within the model of hopping conductivity as developed by Mott.[18] Since the high-temperature Arrhenius behavior and the low-temperature $\ln\rho\propto T^{1/4}$ law (see Fig. 3) are limiting cases of the same mechanism, the apparently metallic conductivity in between might also be of principally semiconducting nature. The positive temperature coefficient should then be brought about by the rapid evolution of the hopping parameters within the narrow temperature regime, in which the PM-FM and FM-AFM transitions take place. Conductivity based on Mott hopping is described by:

$$\sigma = e^2R^2\nu_{\mathrm{Ph}}N(E_F)\exp(-2R/L - W/k_BT). \qquad (1)$$

Here R is the mean hopping distance, L the carrier localization radius, and W the splitting between energy levels related by a hopping process. For the phonon frequency we assumed $\nu_{\mathrm{Ph}}=10^{13}$ Hz, and the density of states was approximated by the free electron model with $N(E_F)=(m^\star/\hbar^2\pi^2)(3\pi^2n)^{1/3}$.[11] The carrier concentration n is supposed to be 0.5 carriers per chemical unit cell, according to the doping ratio with $Pr^{3+}/Sr^{2+}=1/1$, i.e., $9\times10^{21}/\mathrm{cm}^3$. Since we are dealing with a strongly correlated system, the unknown effective carrier mass $m^\star$ was approximated by 10 m_e.

In the paramagnetic state, the Arrhenius plot of resistivity is strictly linear (above 280 K) and W is therefore given by the constant Arrhenius slope. For the mean hopping width R one can assume 3/2 times the distance between adjacent Mn sites, because hopping in a given direction is only allowed between Mn^{3+} and Mn^{4+}, occupying the Mn sublattice randomly for $T>T_C$. Inserting this together with the measured resistivity into Eq. (1), one obtains a carrier localization length of L = 46 Å, thus indicating a considerable smearing of wave functions. The temperature dependence of the parameters W, R, and L is plotted in Fig. 5. Extending this analysis below 280 K, the energy barrier starts to decrease with the occurence of first ferromagnetic fluctuations, accompanied by a rapidly decreasing localization length.

For the regime below 160 K, where the $\ln\rho\propto(\Theta/T)^{1/4}$ scaling holds, we made use of the low-temperature approximations $W=3/[4\pi R^3N(E_F)]$ and $2/L=9/[4\pi R^4N(E_F)k_BT]$ for Eq. (1).[18] This allows us to evaluate the mutually dependent parameters R, L, and W self-consistently without further assumptions. The absolute value for the hopping distance at 160 K corresponds very well to the postulated nearest-neighbor hopping at high temperatures, and exhibits the pronounced low-temperature increase typical for the VRH mechanism (see Fig. 5). Especially the reasonable value for R gives *a posteriori* confidence in the somewhat arbitrarily chosen values for the parameters $m^\star$ [i.e., $N(E_F)$] and ν_{Ph}.[19] The localization length stabilizes at the nearly constant value of 10 Å indicating a carrier localization within roughly three unit cells of the perovskite lattice. We note that this confinement of carriers is at least in a qualitative agreement with the idea of charge ordering, despite that Wigner crystallization in a strict sense was not found according to Sec. IV B 1. The sharp increase of L below 30 K reflects a low-temperature resistivity increase slower than the prediction of pure variable range hopping (Fig. 3), and cannot be interpreted in a straightforward way. Presumably it is associated with magnetic ordering in the Pr^{+3} sublattice. An interesting result is the nearly vanishing hopping barrier below 160 K. The increasing (anti)ferromagnetic order is supposed to bring about, via the high fields on atomic scale, a considerable widening of the energy levels within localized states. Therefore hopping between different localized states will be strongly enhanced, as the netto interstate energy barrier loses importance. The temperature dependence of the barrier in this temperature regime follows the scaling $W(T)\approx1.65T^{3/4}$, where the exponent 3/4 is in precise agreement with the VRH concept.[18]

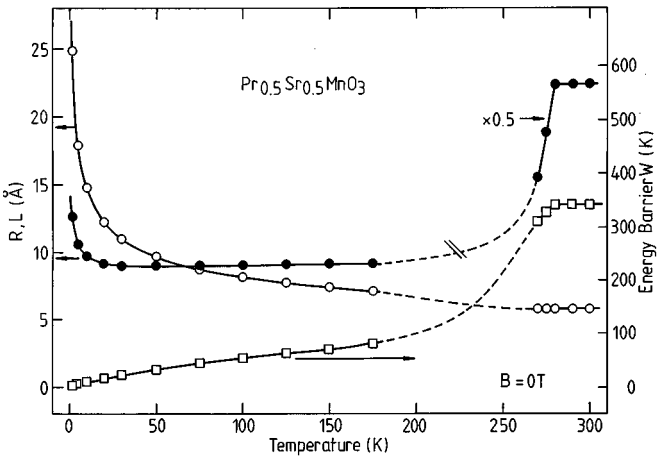

FIG. 5. Temperature dependence of the energy barrier W (□), the mean jump width R (○), and the localization length L (●) in the framework of Mott's hopping concept. The dashed lines suggest a temperature dependence of the three parameters in the metallic transition regime. Note especially the low-temperature increase of R, the enhanced carrier localization in the antiferro- compared to the paramagnetic state, and the almost vanishing hopping barrier for the magnetically ordered phase.

V. RESISTIVITY IN EXTERNAL MAGNETIC FIELDS

A. Experimental results

The influence of external magnetic fields on the resistivity together with the corresponding magnetoresistivity ratios $[\rho(B)-\rho(B=0)]/\rho(B)$ is shown in Fig. 6. Contrary to the

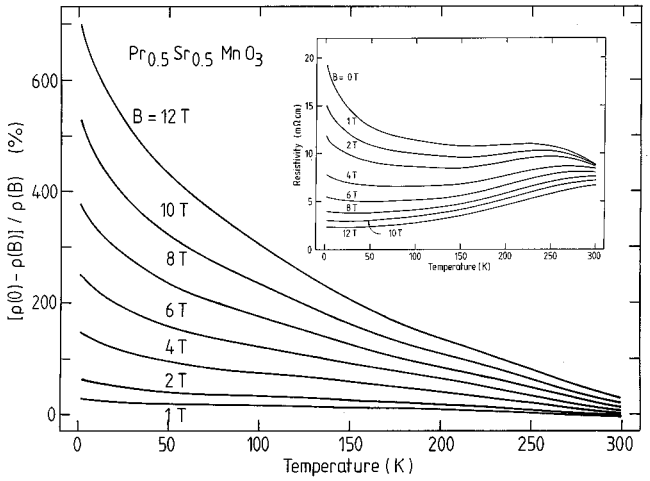

FIG. 6. Temperature dependence of the magnetoresistivity ratio $[\rho(B)-\rho(B=0)]/\rho(B)$ for different external fields $\vec{B}$ parallel to the transport current and perpendicular to the $\vec{c}$ axis. The temperature dependence of the restivity is given in the inset.

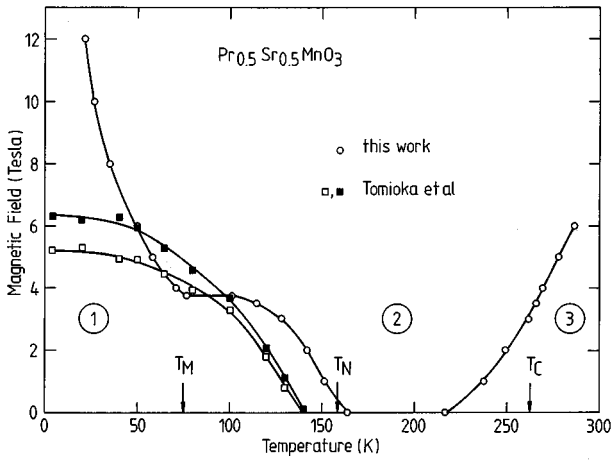

FIG. 7. Splitting of the $B(T)$ phase diagram into three regions of different conductive (magnetic) behavior: Region (1) represents the semiconducting-antiferromagnetic phase with $T_M=75$ K, indicating the maximum temperature for the occurence of the memory effects (Ref. 17). Region (2) stands for metallic-ferromagnetic behavior and (3) for the semiconducting-paramagnetic state. $T_N=158$ K and $T_C=263$ K are the Néel and Curie temperatures, determined from the magnetization data (at 20 mT) in Fig. 2. The temperatures of the charge-liquid to charge-crystal transition and of the inverse transition according to the work of Tomioka *et al.* (Ref. 10) are given by □ and ■, respectively.

doped La manganites, the GMR maximum is not located in the vicinity of the ferromagnetic Curie temperature (in this $Pr_{0.5}Sr_{0.5}MnO_3$ sample at 263 K ± 3 K), but is continuously increasing with decreasing temperature and increasing field, up to 700% for 1.5 K at 12 T. The GMR effect seems to originate not only from the lowering of the resistivity itself, but also from the shifts of the high-temperature semiconductor-metal transition and the low-temperature metal-semiconductor transition to higher and to lower temperatures, respectively. This results in a significant broadening of the metalliclike region, see region (2) in the tentative phase diagram in Fig. 7. The data points of Fig. 7 correspond to the temperatures at the local maxima and minima of the resistivity curves from Fig. 6, in the sense defined for zero field in the inset of Fig. 3. There is also a clear correspondence between the resistively determined transition temperatures and the characteristic temperatures from the magnetization measurements: The boundary between the paramagnetic-semiconducting and the metallic regime follows the field dependence of the inflection point of $M(T)$ (Fig. 2), while the transition from the metallic to the antiferromagnetic-semiconducting phase agrees also with T_N from Fig. 2. The T_C value from the extrapolation $M^{-1}\rightarrow 0$, i.e., 263 K, is considerably above the respective temperature from the resistivity measurements (220 K), but indicates precisely the appearance of first deviations from nearest-neighbor hopping conductivity, as shown in Fig. 3. It is worth mentioning that the two boundary lines in Fig. 8 should not be considered as phase boundaries in a strict sense, because the relevant temperatures might exhibit a certain smearing within the sample volume due to slight local variations of the actual sample composition. For reasons of comparison Fig. 7 shows also the data for the hysteretic, first-order charge-liquid to charge-solid transition as determined by resistive measurements on a single crystal by Tomioka and co-workers.[10]

Resisistivity measurements at fixed temperatures are shown in Fig. 8. Each curve consists of four field sweeps in the sense 0 T→12 T→0 T→−12 T→0 T, starting with a zero-field cooled sample. The curves for 50 K, 100 K, and 150 K exhibit a splitting due to hysteresis which becomes even more pronounced at 5 K. The data at 5 K are omitted in Fig. 8, since the memory effect at low temperatures leads to further complications in interpreting the $\rho(B)$ changes.[17] From the difference in curvature of the $\rho(B)$ data at 298 K and the lower-temperature data, we may conclude that a different GMR mechanism is present in the paramagnetic and the ordered states. Double logarithmic plots of the field induced conductivity versus field revealed the empirical scaling:

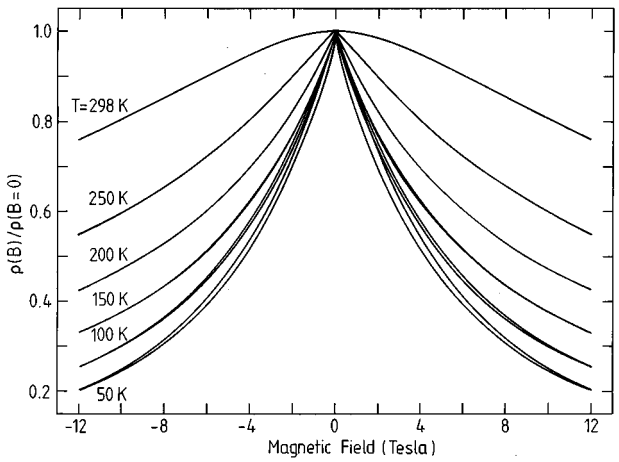

FIG. 8. Field dependence of the magnetoresistivity at different temperatures. The curvature is positive for 298 K and negative for all temperatures below, indicating a unique GMR mechanism for $T\leqslant 250$ K. Hysteretic behavior is visible up to 150 K, with coercitive fields below 100 mT.

$$\sigma(B,T)=\sigma(B=0,T)+\sigma^{\star}(T)\cdot B^{\alpha}. \quad (2)$$

At 298 K the exponent $\alpha\approx 1.82$, a value close to 2, which was reported for the scattering of charge carriers by independent spins.[20,21] For all other temperatures up to 250 K, α varies between 0.99 and 1.20, while systematic deviations appear in the antiferromagnetic phase. Especially at 200 K, still in the ferromagnetic phase, where with increasing field no phase transition line is crossed (see Fig. 7), the conductivity increase remains strictly linear for fields as high as 25 T.[17] At all other temperatures the field-induced shift of transition temperatures, i.e., the crossing of phase-boundary lines, makes a universal scaling more difficult, ignoring already the additional hysteresis effects in the antiferromagnetic phase. It should also be pointed out that the scaling with Eq. (2) can only be a low field approximation, in the sense that saturation tendencies of the GMR effect, especially visible at the low-temperature curves of Fig. 8, are *a priori* not taken into account.

B. The GMR effect and hopping conductivity of magnetic polarons

To interpret the magnetoresistance data, it is worth considering a simple model of hopping conductivity of *magnetic* polarons. In this case the characteristic energy difference W_{ij} between the two levels taking part in an elementary hopping process is dependent upon the relative misorientation of the two local magnetization vectors $\vec{M}_i$ and $\vec{M}_j$. Therefore the energy W_{ij} should be renormalized due to the misfit of the orientations of $\vec{M}_i$ and $\vec{M}_j$ (Fig. 9):

$$W_{ij}\rightarrow W_{ij}-\overline{(\vec{M}_i\cdot\vec{M}_j)}=W_{ij}-\Delta W_{ij}^{s}. \quad (3)$$

In other words, GMR for the hopping conductivity of magnetic polarons appears as a result of the field-induced suppression of an average misorientation between their two local magnetizations $\vec{M}_i$ and $\vec{M}_j$.

In the paramagnetic phase, when the internal Weiss field H_W is absent ($H_W=0$) the average $\overline{(\vec{M}_i\cdot\vec{M}_j)}$ can be approximated by the square of the magnetization M_z along the field axis, resulting in the parabolic GMR effect in low fields.[22] The typical misorientation angle $\Theta\approx 2\varphi_0$ (Fig. 9) depends on φ_0, where φ_0 determines the average projection of $M_z=M\cos\varphi_0$, which is normally described by the Brillouin function. Since $\cos\Theta\approx\cos 2\varphi_0=2\cos^2\varphi_0-1$ one can expect that in the paramagnetic phase the ratio $\Delta\rho/\rho$ should be related to $\cos^2\varphi_0$ and therefore to the square of the Brillouin function.

In the ferro- or antiferromagnetic phase the high internal Weiss field H_W is superimposed with an applied external field H_a. We think that in our case $H_a\ll H_W$ and therefore we may assume that at the two sites (i and j), connected by an elementary hopping process, the external field H_a affects the magnetization only to the minor corrections $\delta M_i,\delta M_j\ll M_W$. The ''main'' magnetization M_W is fully controlled by the Weiss field $H_W\gg H_a$ and therefore not influenced by H_a. Then the correction ΔW_{ij}^{s} due to the spin misorientation of the polarons is

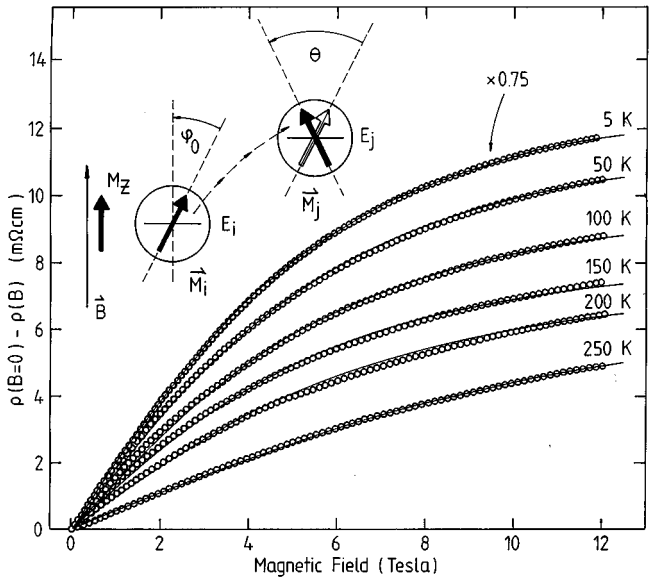

FIG. 9. Comparison of the negative magnetoresistivity $\rho(B=0)-\rho(B)$ with the Brillouin function $A(T)\cdot\mathcal{B}(g\mu_B JB/k_BT)$, plotted as thin solid lines. Deviations occur at 150 K and 200 K, while the coincidence is striking for the other temperatures. The inset represents the hopping process between magnetically ordered clusters of different orientations $\vec{M}_i$ and $\vec{M}_j$ (bold arrows). The typical angle Θ between the orientation of the two polarons is approximated by two times the average misorientation angle of one polaron with the direction of the external field $\vec{B}$.

$$\Delta W_{ij}^{s}=\overline{(\vec{M}_W+\delta\vec{M}_i)\cdot(\vec{M}_W+\delta\vec{M}_j)}$$
$$\approx\vec{M}_W\cdot\vec{M}_W+\vec{M}_W\cdot\overline{(\delta\vec{M}_i+\delta\vec{M}_j)}. \quad (4)$$

It seems to be reasonable to expect that the average of the minor corrections δM_i and δM_j, which follow the applied field H_a, may be described by the Brillouin function. The application of this simple model (based on the *assumption* that only δM_i and δM_j, and not M_W, are influenced by H_a) reveals a striking correspondence between the negative magnetoresistivity and the Brillouin function $\mathcal{B}$ (see Fig. 9) for temperatures below T_C:

$$\rho(B=0,T)-\rho(B,T)=A(T)\cdot\mathcal{B}[g\cdot\mu_B\cdot J(T)\cdot B/k_BT]. \quad (5)$$

Here $A(T)$ and $J(T)$ are the fitting parameters for the amplitude of the negative magnetoresistivity and the spin moment, respectively. Assuming a gyromagnetic ratio $g=2$ for the manganese ions (their spins are 3/2 and 2) one obtains a weakly temperature dependent amplitude factor $A(T)$ and total spin moments $J(T)\approx 45$ in the ferromagnetic regime, see Fig. 10. Upon entering the antiferromagnetic phase at lower temperatures the total moment is decreasing rapidly as it can be expected for a predominant antiparallel alignment of neighboring spins. The dimension of magnetically ordered clusters, thus polaronlike spin arrangements, is calculated straightforwardly in the ferromagnetic regime, resulting in roughly 26 Mn ions, or extending over a cube with a side length of almost three times the chemical unit cell. This is in a remarkable correspondence with the typical carrier localization length $L\approx 9.1$ Å as calculated in Fig. 5. (Here we

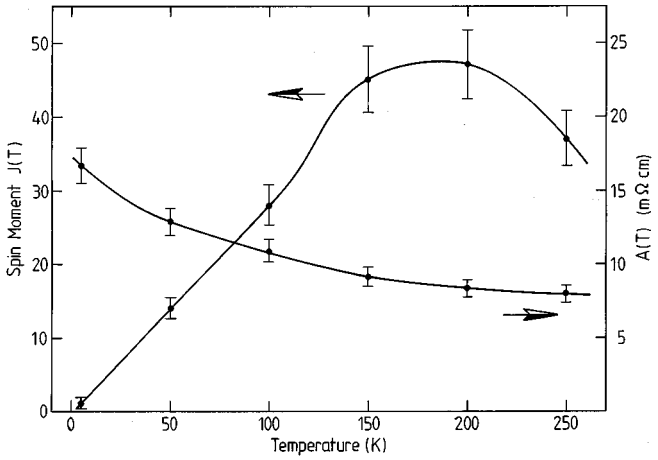

FIG. 10. Temperature dependence of the fitting parameters $A(T)$ (right scale) and $J(T)$ (left scale) from Fig. 9, including typical error bars. The spin moment $J(T)$ approximates in the ferromagnetic state the size of magnetic polarons. Note the rapid decrease of the polaron moment upon entering the antiferromagnetic phase. At the onset of ferromagnetic correlations (250 K) the polarons are also smaller than in the fully developed ferromagnetic state at, e.g., 200 K.

refer to the L value for 150 K, at the onset of antiferromagnetic order, because the hopping analyis does not apply to the ferromagnetic regime itself.) Best agreement of $\mathcal{B}$ with the data in Fig. 9 was achieved at 250 K, close to the ferromagnetic transition, and slight deviations occur at 200 K and 150 K. Deviations from the ideal Brillouin scaling might be related to a certain dependence of the carrier localization length on the external magnetic field, which was experimentally verified for weakly doped GaAs semiconductors.[23] In the purely antiferromagnetic regime, between 5 K and 100 K, the correspondence of the Brillouin function with the data is again very convincing. For these temperatures we analyzed the upper branches of the hysteretic $\rho(B)$ curves, but the scaling works equally well for the lower branches, giving slightly lower amplitude factors $A(T)$.

VI. CONCLUSIONS

Thin films of $Pr_{0.5}Sr_{0.5}MnO_3$ were prepared *in situ* with strong $\vec{c}$-axis orientation, and are characterized with respect to morphology and surface properties. The zero-field resistivity showed semiconducting behavior according to nearest-neighbor hopping in the paramagnetic, and variable range hopping in the antiferromagnetic state. Quasimetallic conductivity was only observed in the temperature regime between 160 K and 220 K, where magnetization measurements reveal a ferromagnetic state. The temperature range of ferromagnetic ordering, and the associated metallic conductivity, become more extended by application of external magnetic fields, which is the first reason for the GMR effect in $Pr_{0.5}Sr_{0.5}MnO_3$. The second reason for GMR is a global lowering of resistivity, which can be scaled with the Brillouin function. From (i) the applicability of the Brillouin function and (ii) the involved fitting parameters we conclude for the ferromagnetic state the existence of magnetic polarons, polarizing the spins of 20 – 30 manganese ions, which become aligned through the external fields. This alignment reduces the hopping barrier and enhances the charge transport. The localization length is of the order of the size of magnetic polarons.

The GMR mechanism in the antiferromagnetic state appears to be of a similar origin as for the ferromagnet, since both obey in good approximation the same scaling laws. This is irrespective of whether we consider the Brillouin scaling for the resistivity decrease or the power-law scaling for the conductivity increase. From the spin moments in the antiferromagnetic state it is however not possible to calculate the cluster sizes as simply as for the ferromagnetic phase. This is because these moments might equally well shrink due to improved antiparallel spin alignment at low temperatures, or due to a decreasing number of Mn ions involved in the formation of these magnetic polarons. The external field generates in any case a (small) parallel component of initially antiparallel oriented spins in the direction parallel to the applied field and enhances the spin dependent charge transport. In the low-temperature limit of the AFM phase, where the spin lattice is most perfectly developed, the fitted spin moment for a polaron collapses to the value of an individual Mn ion, which gives additional confidence to the presented idea of a GMR effect based on field-induced reduction of the misalignment of magnetic polaron moments.

We would also like to point out that for potential field sensing purposes it seems to be more interesting to use antiferromagnetic compounds like $Pr_{0.5}Sr_{0.5}MnO_3$ since they exhibit GMR not only around the ferromagnetic transition temperature, but at all temperatures below room temperature.

ACKNOWLEDGMENTS

This work is financially supported by the Belgian National Fund for Scientific Research (NFWO), the Inter-University Attraction Poles Programmes, and the Flemish Concerted Action Programme. L.T. thanks the Vlaams Instituut voor de Bevordering van het Wetenschappelijk-Technologisch Onderzoek in de Industrie for financial support. Technical assistence by R.J.M. Vullers, M. Van Bael, and L. Parys is gratefully acknowleged. We are indebted to G. Jakob, M. Verwaest, E. Rosseel, and L. Miu for interesting discussions and valuable experimental advice.

*Present address: Materials Science Division, Argonne National Laboratory, 9700 South Cass Avenue, MSD/223, Argonne, IL 60439-4845.

[1] G. H. Jonker and J. H. Van Santen, Physica **16**, 337 (1950); **16**, 599 (1950).

[2] R. von Helmolt, J. Wecker, B. Holtzapfel, L. Schultz, and K. Samwer, Phys. Rev. Lett. **71**, 2331 (1993).

[3] R. M. Kusters, J. Singleton, D. A. Keen, R. McGreevy, and W. Hayes, Physica B **155**, 362 (1989).

[4] S. Jin, M. O'Bryan, T. H. Tiefel, M. McCormack, and W. W. Rhodes, Appl. Phys. Lett. **66**, 382 (1995).

[5] C. Zener, Phys. Rev. **82**, 403 (1951).

[6] P. W. Anderson and H. Hasegawa, Phys. Rev. **100**, 675 (1955).

[7] P. G. de Gennes, Phys. Rev. **118**, 141 (1960).

[8] M. F. Hundley, M. Hawley, R. H. Heffner, Q. J. Jia, J. J. Neumeier, J. Tesmer, J. D. Thompson, and X. D. Wu, Appl. Phys. Lett. **67**, 860 (1995).

[9] K. Knížek, Z. Jirák, E. Pollert, F. Zounová, and S. Vratislav, J. Solid State Chem. **100**, 292 (1992).

[10] Y. Tomioka, A. Asamitsu, Y. Moritomo, H. Kuwahara, and Y. Tokura, Phys. Rev. Lett. **74**, 5108 (1995).

[11] N. W. Ashcroft and N. D. Mermin, *Solid State Physics* (Saunders College, Philadelphia, 1976).

[12] P. Wagner, F. Hillmer, U. Frey, H. Adrian, T. Steinborn, L. Ranno, A. Elschner, I. Heyvaert, and Y. Bruynseraede, Physica C **215**, 123 (1993).

[13] Especially in the cooling runs the magnetization is not vanishing for $T \rightarrow 0$. This means that the ideal AFM spin structure might be modified by a canting of sublattices.

[14] A. Kebede *et al.*, Phys. Rev. B **40**, 4453 (1989); I. Felner *et al.*, *ibid.* **40**, 6739 (1989).

[15] T. F. Conolly and E. D. Copenhaver, *Bibliography of Magnetic Materials and Tabulation of Magnetic Transition Temperatures* (IFI Plenum, New York, 1972).

[16] E. F. Bertaut, G. Buisson, A. Durif, J. Mareschal, M. C. Montmory, and S. Quezel-Ambrunaz, Bull. Soc. Chim. France Vol. **1**, 1132 (1965).

[17] J. Vanacken, P. H. Wagner, G. Kido, V. V. Moshchalkov, and Y. Bruynseraede (unpublished).

[18] N. F. Mott and E. A. Davis, *Electronic Processes in Non-Crystalline Materials* (Clarendon Press, Oxford, 1979).

[19] The assumed values for ν_{Ph} and $m^{\star}$ are comparatively high. Lower values however would increase the evaluated carrier localization lengths and jump widths above the physically reasonable nearest-neighbor hopping.

[20] J. Z. Sun, L. Krusin-Elbaum, S. S. P. Parkin, and X. Xiao, Appl. Phys. Lett. **67**, 2726 (1995).

[21] G. C. Xiong, Q. Li, H. L. Ju, S. M. Bhagat, S. E. Lofland, R. L. Greene, and T. Venkatesan, Appl. Phys. Lett. **67**, 3031 (1995).

[22] J. Inoue and S. Maekawa, Phys. Rev. B **53**, R11927 (1996).

[23] J. L. Pichard, M. Sanquer, K. Slevin, and P. Depray, Phys. Rev. Lett. **65**, 1812 (1990).

[24] H. Yoshizawa, H. Kawano, Y. Tomioka, and Y. Tokura, Phys. Rev. B **52**, 13 145 (1995).